Dendrochronologia 92 (2025) 126343

Contents lists available at ScienceDirect

Dendrochronologia

journal homepage: www.elsevier.com/locate/dendro

X-ray micro-CT pipeline for large-scale tree-ring densitometry studies

Louis Verschuren [a,b,c,*], Vladimir Matskovsky [a,b], Matthieu N. Boone [b,d], Luc Van Hoorebeke [b,d], Joris Van Acker [a,b], Tom De Mil [e], Valerie Trouet [f], Charlotte Pearson [f], Jorden De Bolle [b,g], Toon Gheyle [a,b], Jan Van den Bulcke [a,b]

[a] UGent-Woodlab, Department of Environment, Faculty of Bioscience Engineering, Ghent University, Coupure links 653, Ghent 9000, Belgium
[b] UGent Centre for X-ray Tomography (UGCT), Ghent University, Proeftuinstraat 86/N12, Ghent 9000, Belgium
[c] Forest & Nature Lab, Department of Environment, Faculty of Bioscience Engineering, Ghent University, Geraardsbergsesteenweg 267, Melle 9090, Belgium
[d] UGent-Radiation Physics, Department of Physics and Astronomy, Ghent University, Proeftuinstraat 86/N12, Ghent 9000, Belgium
[e] Forest is life, TERRA Teaching and Research Centre, Gembloux Agro-Bio Tech, University of Liège, Passage des Déportés 2, Gembloux 5030, Belgium
[f] Laboratory of Tree Ring Research, University of Arizona, 1215 E Lowell St., Tucson, AZ 85721, USA
[g] Deptartment of Solid State Sciences - CoCooN research group, Faculty of Sciences, Ghent University, Krijgslaan 281 / S1, Ghent 9000, Belgium

ARTICLE INFO

Keywords:
X-ray micro-computed tomography
Tree-ring densitometry
Maximum latewood density
Helical XμCT
Dendrochronology

ABSTRACT

Tree-ring data provides essential insights into historical climate conditions and current ecosystem dynamics. Wood density measurements complement traditional tree-ring width series by extracting additional climatic information embedded within tree rings, with maximum latewood density serving as the gold standard for summer temperature reconstructions. However, the labor-intensive wood sample preparation required by conventional techniques is one of the main factors limiting the more widespread use of tree-ring densitometry. X-ray micro-computed tomography (XμCT) offers a novel, non-destructive, 3D densitometry technique that enables the simultaneous study of tree-ring width and wood density at high resolution and with minimal sample preparation. Despite its potential, the lack of a streamlined and time-efficient XμCT workflow has hindered its broader application in the past. Here we present a highly optimized XμCT pipeline aimed at large-scale tree-ring densitometry studies, capable of processing large amounts of increment cores with a low demand for human labor time (2.2–5.4 min per 35 cm sample length). Key parts include large and efficient sample holders (16–48 samples per scan), optimized and standardized scan settings (helical XμCT at 15, 30, and 60 μm voxel size), and three custom software packages (facilitating scan processing, ring indication, and cross-dating). Overall, this XμCT toolchain represents a significant leap forward in high-resolution tree-ring densitometry, enabling large-scale studies with a wide spatial extent, high replication, and/or long temporal range.

1. Introduction

Tree-ring data offers valuable insights into historical climate conditions (Briffa, 1999; Jones et al., 2009; Björklund et al., 2023) and current ecosystem dynamics (Swetnam et al., 1999; Babst et al., 2019). In addition to the traditional tree ring width (TRW) series, the use of wood density measurements has long been a significant asset in extracting climate signals embedded within these tree rings (Briffa et al., 2004). For example, maximum latewood density (MXD) measurements from X-ray-based microdensitometric data serve as the gold standard for summer temperature reconstructions (Wilson and Luckman, 2003; Esper et al., 2012; Bjorklund et al., 2014; Wilson et al., 2016; De Mil et al., 2024). In conifers, temperature affects the thickness of latewood cell walls formed at the end of the growing season, resulting in fluctuating MXD values (Björklund et al., 2017). Densitometry of increment cores has also shown to be a valuable tool in quantifying carbon dynamics in forests, since density is an important variable for biomass estimations (Chave et al., 2014; Vannoppen et al., 2018; Hubau et al., 2019).

Büntgen and Esper (2024) call for the development of large paleo-climatic proxy archives with a high spatial resolution to robustly investigate trends and extremes in the Earth's surface temperature. However, the use of tree-ring densitometry for such large-scale studies is currently limited by the laborious wood sample preparation needed with conventional X-ray-based techniques (Schweingruber et al., 1978). X-ray micro-computed tomography (XμCT) is a novel, non-destructive, 3D densitometry technique enabling the simultaneous study of

* Corresponding author.
E-mail address: louis.verschuren@ugent.be (L. Verschuren).

https://doi.org/10.1016/j.dendro.2025.126343
Received 17 January 2025; Received in revised form 17 March 2025; Accepted 27 April 2025
Available online 30 April 2025

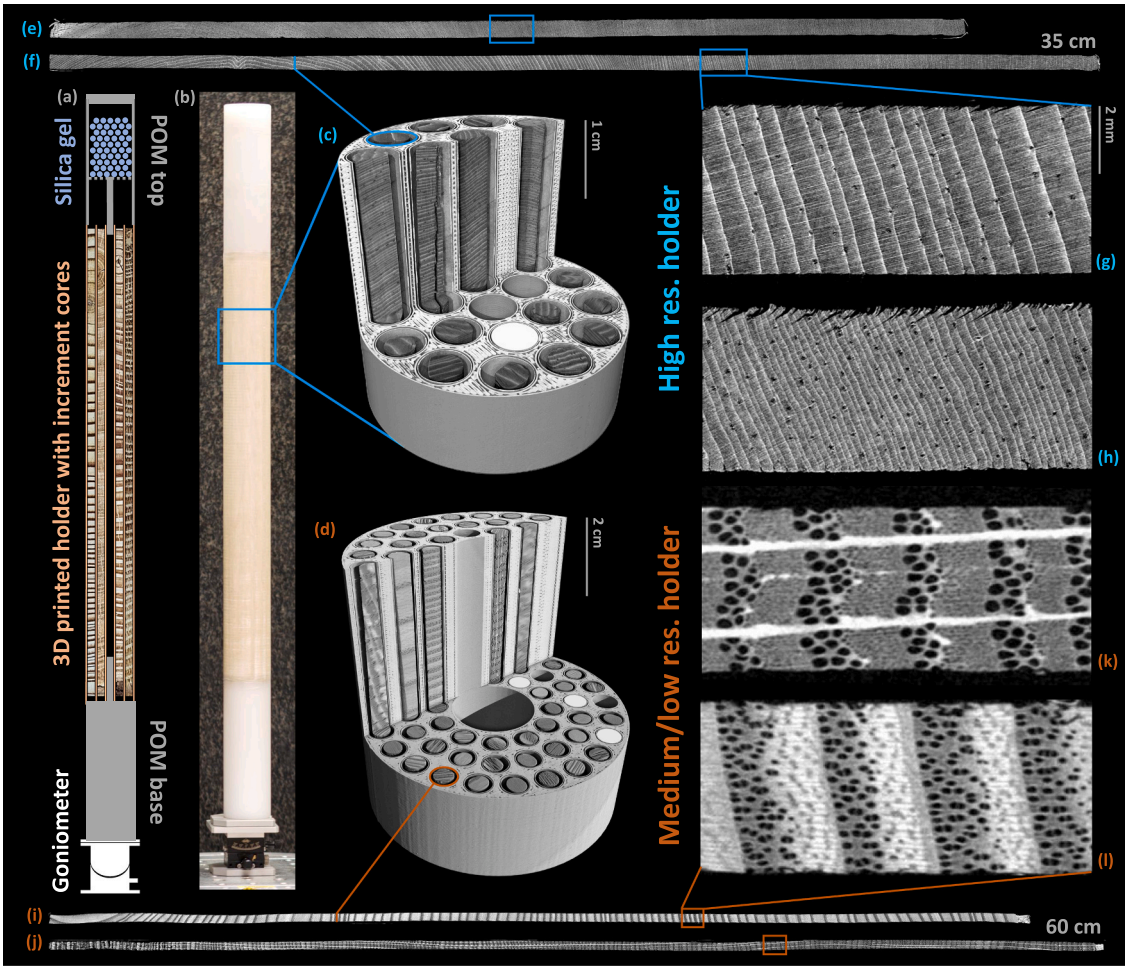

Fig. 1. An overview of the two holders and XμCT-scanning results. **(a)** A schematic shows the overall design, including a POM top with integration of silica gel, a 3D printed holder with increment cores, a POM base, and a goniometer for precise positioning. **(b)** Photograph of the high-resolution holder. **(c)** XμCT scan 3D rendering from the high-resolution holder (3 cm section of 35 cm scan). This holder can accommodate 16 increment cores up to 35 cm in length. **(d)** XμCT scan 3D rendering from the medium/low-resolution holder (6 cm section from 60 cm scan). This holder can accommodate 48 increment cores up to 60 cm in length. **(e)** and **(f)** are high-resolution increment core scans (15 μm voxel size) from *Pinus longaeva* D.K.Bailey, with **(f)** having a length of 35 cm. **(g)** and **(h)** are zoomed in sections of these high resolution scans. **(i)** and **(j)** are medium resolution increment core scans (30 μm voxel size) from *Fraxinus excelsior* L. and *Quercus robur* L. respectively, with **(j)** having a length of 60 cm. **(k)** and **(l)** are zoomed in sections of these medium resolution scans.

tree-ring width and wood density while requiring little sample preparation (Van den Bulcke et al., 2019). It could allow for high-throughput tree-ring densitometry studies with large sample sizes and limited preparation time. Despite its potential, the lack of a streamlined and time-efficient XμCT workflow has hindered its broader application in the past.

Here we present a highly optimized XμCT pipeline aimed at large-scale tree-ring densitometry studies, capable of processing large amounts of increment cores at high resolution while having low labor time requirements. Key parts include (1) large and efficient 3D-printed sample holders; (2) optimized and standardized scan settings; (3) helical XμCT reconstruction with corrected heel artifacts; (4) user-friendly software packages (building further on Van den Bulcke et al. 2014 and De Mil et al. 2016) that can handle very large scan sizes (available at www.dendrochronomics.ugent.be). Additionally, we scanned a set of reference wood samples with known density to check the accuracy of XμCT density estimates, compare scan settings, and enable multi-scanner use. This toolchain is the result of more than 10 years of development at UGent-Woodlab (De Ridder et al., 2011; Van den Bulcke et al., 2014, 2019; De Mil et al., 2016; Vannoppen et al., 2017; De Mil and Van den Bulcke, 2023) and aims to be the leading platform for XμCT-based tree-ring densitometry. The presented pipeline makes high-resolution tree-ring densitometry accessible for large-scale studies with a wide spatial extent, high replication, and/or very long temporal range.

2. Sample holders

Here we present two sample holders that are designed to hold standard 5 mm increment cores: a high-resolution holder and a medium/low-resolution holder, both featuring a similar design (see Figure 1). Each holder consists of three parts. The top part is a hollow POM (Polyoxymethylene) end cap that contains silica gel to keep the air inside the holder dry, as samples are oven-dried (103 ˚C, 24 h) before scanning to enhance reproducibility and compatibility between studies. The middle section is a 3D-printed ABS (Acrylonitrile Butadiene Styrene) sample holder that accommodates increment cores and density references. Standard 5 mm increment cores (or smaller) are stored in 6 mm paper straws (Artstraws®), which friction fit in the 7 mm sample holder holes. A POM base fits on the bottom of the holder. This holder includes a metal base plate with magnets which allows for secure attachment to a goniometer, facilitating precise vertical alignment of the holder. The central cavity of the holder is used to connect the top and bottom using a protruding POM rod. This creates a straight cylinder shape with a constant diameter. Parafilm is used to seal the connections between parts during the scanning process. This is done to keep air from

Table 1
Overview of the scan settings used for the four scan modes: high resolution fast, high resolution optimal, medium resolution, and low resolution. SDD stands for Source Detector Distance, SOD for Source Object Distance. As the two holders have a different length and numbers of increment cores, the scan time per 35 cm of increment core is also shown.

	High res. fast	High res. optimal	Medium res.	Low res.
Voxel size (μm)	15	15	30	60
Smooth or step-and-shoot scan	smooth	step-and-shoot	smooth	smooth
Exposure time per projection (ms)	180	1400	360	180
Power (W)	15	15	30	60
Voltage (kV)	100	100	100	100
SDD (mm)	600	600	600	600
SOD (mm)	60	60	120	120
Projections per turn	4075	4075	4075	2037
Detector binning mode	1	1	1	2
Aluminium filter thickness (mm)	0.5	0.5	0.5	0.5
Samples per scan	16	16	48	48
Holder length (cm)	35	35	60	60
Scantime full holder (min.)	82	1440	140	34
Scantime per 35 cm sample (min.)	5.13	90.00	1.57	0.38

entering the holder during a scan.

The high-resolution holder has a diameter of 39 mm and can accommodate 16 increment cores, each up to 35 cm in length. This length covers the average range of the majority of cores collected for dendrochronological studies, lowering the need to split cores into multiple sections. The holder also includes one air reference (an empty hole, 0.0012 g/cm^3) and one POM reference rod. POM has a homogeneous density of 1.41 g/cm^3 and a similar atomic composition as wood cell walls (Moonen et al., 2022). With this high-resolution holder, a voxel size of 15 μm can be achieved in a commercially available XμCT system (TESCAN CoreTOM, see section 3). The medium/low-resolution holder, with a diameter of 74 mm, can hold up to 48 increment cores, each up to 60 cm in length. This holder includes three air references and three POM references, and a voxel size of 30 μm can be obtained. The sample locations within the holders are based on a mathematically optimal packing, maximizing spatial efficiency (Lubachevsky and Graham, 1997; Fodor, 1999). This circular shape with internal circular symmetry has the added benefit of avoiding streaking artifacts, typically seen in CT-images around sharp edges. The use of 3D-printing technology allows for a consistent minimal wall thickness of 0.8 mm and ensures long straight holes, which is not feasible with traditional manufacturing methods. Dense packing and thin walls result in a large amount of samples fitting inside a small cross-sectional area. This makes scanning of a large number of samples at a high resolution not just technically feasible, but practically viable.

Larger diameter increment cores can easily be accommodated by designing new sample holders using the same basic design. The most important feature to consider for new holder specifications is the outer diameter, which dictates the highest achievable voxel size.

3. XμCT-scanner and scan settings

The XμCT scanner used in this paper is a TESCAN CoreTOM (TESCAN, Ghent, Belgium), which is a versatile, general-purpose system. It features a 30–180 kV / 300 W X-ray tube and a large flat panel detector with a resolution of 2856 × 2856 pixels and a pixel pitch of 0.15 mm. All increment core scans are performed in helical mode. In this mode, the object is moved vertically while rotating (relative to the source and detector), following a helical scan trajectory. Helical scanning is perfect for increment cores as it avoids cone beam artifacts, which are particularly problematic for tree rings due to the sharp density changes at the

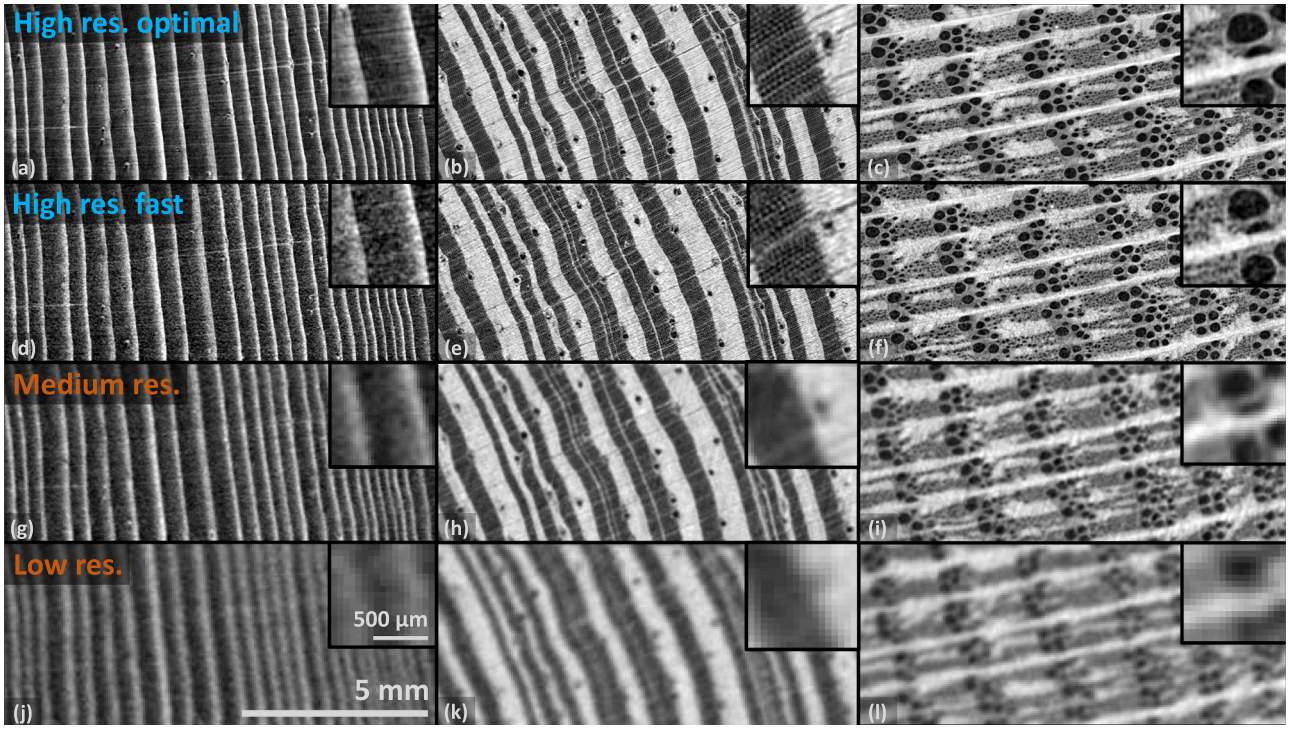

Fig. 2. Three 5 mm increment cores scanned in the four different scan modes: high resolution optimal (15 μm voxel size, 1400 ms exposure time) **(a, b, c)**, high resolution fast (15 μm voxel size, 180 ms exposure time) **(d, e, f)**, medium resolution (30 μm voxel size, 360 ms exposure time) **(g, h, i)**, and low resolution (60 μm voxel size, 180 ms exposure time) **(j, k, l)**. The increment cores are *Picea abies* (L.) H. Karst. **(a, d, g, j)**, *Pinus rigida* Mill. **(b, e, h, k)**, and *Quercus robur* L. **(c, f, i, l)**. A zoomed-in section is shown in each corner. The images display the middle 60 μm of each core in the Z-direction. For the high- and medium-resolution scans, the data were averaged along the Z-axis to ensure the represented volume matches across all images.

Table 2
Compute time needed for normalization, heel correction, and reconstruction of a full 35 cm high-resolution holder (first column) or a 60 cm medium/low-resolution holder (last two rows) helical scan. As these have different lengths and numbers of increment cores, the processing time per 35 cm of increment core is also shown. The final size of the full reconstructed holders and a 35 cm finished core are shown in GB.

	High res. fast/ optimal	Medium res.	Low res.
Normalisation (h.)	0.6	0.5	0.06
Heel correction (h.)	2.0	1.7	0.15
Reconstruction (h.)	47	39	2.7
Total compute time per 35 cm sample (h.)	3.1	0.5	0.035
Reconstructed holder size (GB)	362	310	39
Final core size per 35 cm sample (GB)	5.6	0.7	0.088

ring boundaries and the often horizontal ring boundary orientation when scanning long increment cores (De Witte, 2010; Van den Bulcke et al., 2014). It also removes the need for stitching when scanning long objects such as increment cores. This means only one scan per filled holder is needed, removing overhead time per scan. Our system has a slow minimal vertical speed that enables smooth helical scanning instead of step-and-shoot. During a smooth scan, the object moves upward continuously at a speed limited by the vertical motor axis resulting in faster scan completion but generally shorter exposure times than step-and-shoot, thus increasing noise. In contrast, a step-and-shoot XμCT scan involves the object being scanned in discrete steps, with the movement stopping for each image captured before moving to the next position. This allows for longer exposure times, reducing noise but typically inducing overhead time as the system needs to stabilize after each movement.

An overview of the scan settings, optimized for our scanner and holder combinations, can be found in Table 1. We define these four modes when scanning increment cores: high resolution fast, high resolution optimal, medium resolution, and low resolution (see Figure 2). The high-resolution modes, with a voxel size of 15 μm, are designed for maximum latewood density (MXD) studies on conifers, angiosperm studies with very narrow rings, or studies of species with difficult-to-discern ring boundaries like in many tropical species. The high-resolution fast mode performs a smooth scan with an exposure time of 180 ms per projection and is the best option for most of these studies. It requires 5.13 min of scan time per 35 cm sample (82 min for the full holder). In contrast, the high-resolution optimal mode uses a step-and-shoot approach with an exposure time of 1400 ms, which reduces noise but increases scan time from 5.13 min (smooth) to 90 min (step-and-shoot) of scan time per 35 cm sample (1440 min for the full holder). Medium-resolution scans have a voxel size of 30 μm and are suited for studies on angiosperms or studies on fast-growing conifers with no interest in MXD. The advantage of this mode is the ability to process a larger number of samples per scan (48 samples of 60 cm versus 16 samples of 35 cm), thereby reducing potential costs and operator time. As such, this mode only requires 1.57 min of scan time per 35 cm sample (140 min for the full holder). Additionally, it results in digital increment cores with eight times smaller file sizes than high-resolution scans, which makes them easier to handle. Low-resolution scans, with a voxel size of 60 μm, are intended for studies on increment cores where tree rings are not the main interest, such as carbon stock studies or wood technology studies. They are also an option for studies on trees with consistently wide rings such as plantation forests. These scans are very fast to complete (0.38 min of scan time per 35 cm sample, 34 min for the full holder) and to process, and produce digital increment cores with a 64 times smaller file size than high-resolution scans. A step-and-shoot version of the medium and low-resolution modes is not implemented here as the smooth scans are already close to the optimal exposure time for our detector. Note that a voxel size of 60 μm is typically not seen as a low resolution in XμCT, it is however the minimum we suggest for studies involving tree rings.

Each of the scan settings presented in Table 1 was optimized and rigorously tested to ensure optimal scan quality. The highest resolution, set at a voxel size of 15 μm, is sufficient to resolve most tree rings encountered in dendrochronological studies while allowing for a sample holder of 16 increment cores to fit within the field of view of our detector. For medium- and low-resolution scans, voxel sizes of 30 μm and 60 μm were chosen. These sizes are exact multiples of 15 μm, ensuring compatibility between resolutions when rebinning the data (i.e., grouping smaller voxels into larger ones to match a coarser resolution). These lower resolutions are adequate for most hardwood species while allowing for a larger sample holder with 48 increment cores and more manageable file sizes. The exposure time and number of projections per turn of the three smooth helical modes were chosen to match the vertical speed to the lowest possible vertical speed of the CoreTOM scanner while the vertical motion within one projection is exactly one pixel, inducing only a limited vertical blur. This setup ensures the highest possible exposure time without reducing the resolution due to blurring. The exposure time of the step-and-shoot mode was chosen to be the highest possible without overexposing our detector. A voltage of 100 kV, combined with a 0.5 mm aluminum filter, was chosen as the optimal configuration to achieve high contrast, sufficient signal strength, and minimal beam hardening. This optimal combination was determined through simulations using the *Arion* software (Dhaene et al., 2015) (see Appendix A) and practical testing of selected configurations. The power is set at 15 W, 30 W, and 60 W to maximize the signal without excessively increasing the spot size. At these settings, the system is calibrated to have the spot sizes stay below their respective voxel sizes, resulting in a limited influence of the spot size on the final resolution. A Source Detector Distance (SDD) of 600 mm was chosen as it represents the most compact setup possible with our source and detector combination. For the low-resolution mode, the detector is binned to 1428 x 1428 pixels with a pixel size of 0.3 mm.

This standardized scanning process ensures consistency, and can potentially be applied at multiple laboratories. This would enable fully inter-comparable datasets, thereby enhancing collaborative research efforts. This is something conventional micro-densitometric techniques have historically struggled with (Björklund et al., 2019). Note that other scanners will have different tube specifications, detectors, and vertical speeds, so experimentation will be necessary when using different XμCT systems. This configuration however serves as a good starting point. When experimenting with different scanners, it is strongly recommended to maintain a voxel size of 15 and 30 μm, as metrics such as MXD are highly sensitive to resolution (Jacquin et al., 2017; Björklund et al., 2019). Depending on the detector, this might result in sample holders with different sizes to the ones presented in this paper. Additionally, synchrotron-based XμCT is also an option. Helical scans and heel correction are then not needed, as a parallel beam geometry is used. It would also enable even shorter scan times for similar signal/noise levels. Vertical travel and beam size could however be a problem with larger holders. Also, accessibility to such large-scale facilities is less straightforward.

4. Helical XμCT reconstruction

Scan reconstructions, based on the Katsevich algorithm (Katsevich, 2002), are performed using the *Octopus Reconstruction* software (Dierick et al., 2004; Vlassenbroeck et al., 2007; De Witte, 2010), which provides precise control over reconstruction parameters, demonstrates high stability, and imposes low hardware demands. Alternative reconstruction software packages, either delivered with the XμCT system or standalone, are also an option.

Following normalization, a heel effect correction is applied to the projections. The heel effect arises due to the non-uniform X-ray energy

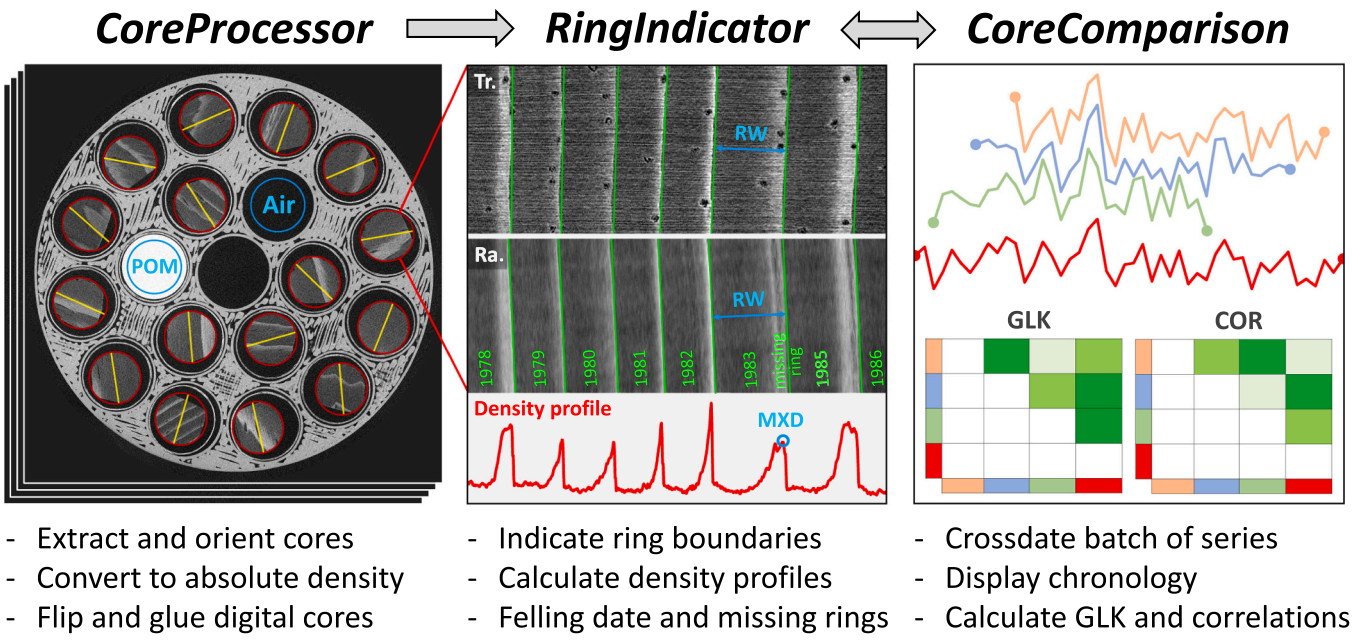

Fig. 3. Schematic representation of the three software packages. *CoreProcessor* (left) extracts image volumes of individual samples from scans (red circles), orients them according to the fiber direction (yellow lines), and converts them to absolute density values using POM and air references (blue). RingIndicator (middle) is used to indicate ring boundaries (in green, both on the transverse (Tr.) and the radial (Ra.) plane) and calculate density profiles (in red). *CoreComparison* (right) facilitates cross-dating by displaying ring-width curves of indicated cores and optional reference chronologies (red). It also calculates inter-series gleichläufigkeit (GLK) and correlation statistics between all loaded series. Note that these are not screenshots of the actual software but rather simplified representations created for visualization purposes.

Table 3
A summary of the approximate human labor time required to process a full sample holder using different scan modes: high-resolution XμCT and medium/low-resolution XμCT.

	High res. fast/ optimal	Medium/low res.
Number of samples per sample holder	16	48
Maximum length of sample (cm)	35	60
Inserting cores into paper straws (min.)	32	96
Loading the holder and filling the Excel template (min.)	10	30
Setting up scan (min.)	15	15
Setting up reconstruction (min.)	10	10
Setting up digital extraction (min.)	5	15
File management and backups (min.)	15	15
Total labor time per sample holder (min.)	87	181
Labor time per 35 cm of sample (min.)	5.4	2.2

spectrum emitted from the X-ray tube, attributed to the anode target's angled geometry inside the tube (Braun et al., 2010). This effect can result in non-uniform imaging, which is particularly important in helical XμCT scans. Correction of the heel effect is achieved using an automated lookup table that adjusts pixel values in the normalized projection images. This lookup table is derived from a POM wedge projection, which simulates varying levels of attenuation at each point along the X-ray beam. Additionally, this method partially mitigates beam hardening effects. For an in-depth explanation of the heel correction methodology, see (De Bolle et al., under review).

The reconstruction and heel correction are performed on a Windows PC with an Intel i7–13700K processor, 64 GB of DDR5 memory, an NVIDIA RTX 3050 GPU, and a 2 TB NVMe SSD. Table 2 details the time required for each step in reconstructing a full holder. Helical reconstruction is notably time-consuming compared to circular scans. Of course, it would be possible to run several of these reconstructions in parallel using multiple Windows virtual machines on a large server, for example.

5. Custom software

The in-house developed *XCT Toolchain* software suite, based on MATLAB (The MathWorks Inc., 2024), consists of three executable programs: *CoreProcessor*, which extracts individual cores from scans and converts them to absolute density values; *RingIndicator*, designed for semi-automatic ring indication and density profile calculation; and *CoreComparison*, which facilitates cross-dating (see Figure 3 for a schematic representation of the three packages). The packages are compiled for Microsoft Windows, and require the free installation of MATLAB Runtime. Comprehensive video manuals and all necessary software are available for free at www.dendrochronomics.ugent.be.

5.1. CoreProcessor

CoreProcessor extracts image volumes of individual samples from scans, orients them according to the fiber direction, and converts them to absolute density values. Since reconstructed XμCT scans in our setup can exceed 300 GB, it is time-consuming and often impractical to load these entire scans into memory. To address this, cores are extracted using a slice-by-slice method. First, 100 evenly spaced slices of the scan are averaged and plotted for manual annotation of locations of the samples and reference pairs. The fiber orientation of each sample is also marked manually. The software then automatically processes each indicated sample by extracting, rotating, and converting it slice-by-slice. Initially, reference curves are generated by extracting the POM (1.41 g/cm^3) and air (0.0012 g/cm^3) reference pairs from each slice. Then, based on available RAM, the program processes a part of the samples, extracting and converting them in batches until all cores in the scan are completed. This approach eliminates the need to load the entire scan into memory at once.

The extraction process also supports the assignment of different air and POM reference pairs to various groups of increment cores. This feature is particularly useful for mitigating the effects of beam hardening, especially in larger holders. The medium/low-resolution holder is typically used with a reference pair for each of the three concentric

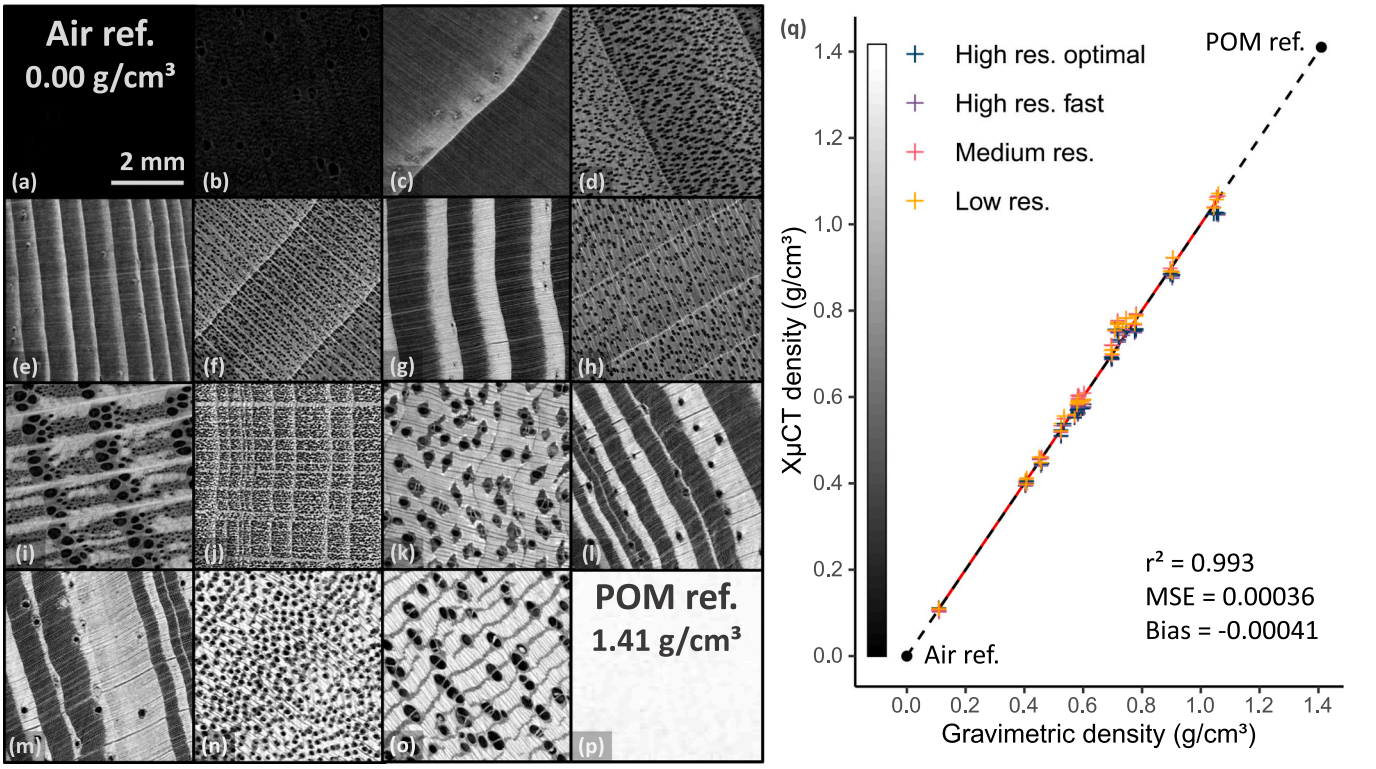

Fig. 4. An overview of the reference samples: a 5×5 mm section of each species, scanned in high-resolution optimal mode, is shown on the left. The samples are ordered by ascending density: **(a)** Air density reference (0.0012 g/cm^3), **(b)** *Ochroma pyramidale* Urb., **(c)** *Picea abies* (L.) H. Karst. fast growth, **(d)** *Populus x canadensis* Moench, **(e)** *Picea abies* (L.) H. Karst. slow growth, **(f)** *Tillia cordata* Mill., **(g)** *Pseudotsuga menziesii* (Mirbel) Franco, **(h)** *Betula pendula* Roth, **(i)** *Quercus robur* L., **(j)** *Fagus sylvatica* L., **(k)** *Afzelia bipindensis* Harms, **(l)** *Pinus rigida* Mill. Soxhlet extracted, **(m)** *Pinus rigida* Mill. not Soxhlet extracted, **(n)** *Handroanthus spp.*, **(o)** *Lophira alata* Banks, and **(p)** POM density reference (Polyoxymethylene, 1.41 g/cm^3). **(q)** A comparison between gravimetric density (ovendry mass/ovendry volume) and XμCT density. The 1:1 line between air and POM is shown dashed in black. The linear fit is shown in red.

groups of samples (see Figure 1). Testing revealed a deviation of 0.015 g/cm^3 between the reference pairs of the inner and outer sample groups due to beam hardening, necessitating a multi-reference approach. In contrast, the high-resolution holder showed a deviation of only 0.001 g/cm^3, making the use of a single reference pair sufficiently accurate.

The file type for extracted cores is signed int16 multi-page BigTIFF (integer representing density in kg/m^3). The traditional Tagged Image File Format (TIFF) is limited to a maximum file size of about 4 GB. In contrast, the BigTIFF format allows for files up to 16 Exabytes (Pennefather and Suhanic, 2009). Using this format is necessary as long cores scanned at 15 μm resolution frequently exceed the 4 GB limit of regular TIFF. Additionally, the use of signed int16 was implemented to accommodate negative density values. Negative density measurements can, for example, occur in samples with large vessels, where the air inside the vessels has a density close to zero (0.0012 g/cm^3). Due to noise, the measured density of air follows a normal distribution around zero. Changing the negative values to zero would overestimate the total density of the sample as only the positive part of the distribution would be retained. The software also uses TIFF tags to define voxel size (resolution), ensuring that the images can be universally understood by other software packages. This, for example, enables easy image manipulation in programs like Fiji (Schindelin et al., 2012). The density value −9999 is used as the NA value, these voxels are automatically removed from the subsequent processing chain by *RingIndicator*. This is for example useful when certain parts of a sample need to be excluded from the density profile.

5.2. RingIndicator

RingIndicator is used to indicate ring boundaries and calculate density profiles. It is custom-made to work with XμCT images but can also be used to measure optical RGB, anatomical masks, multi-spectral images, or any other TIFF image format. Ring boundaries are indicated as lines, both on the transverse and the radial plane of the 3D digital increment core. The indication process is semi-automatic, as borders can be automatically detected using peaks and valleys in the density profile. For each sample, a continuous density profile along the whole length of the core is calculated which accounts for the 3D orientation of the ring boundaries (Van den Bulcke et al., 2014). The user can set the size of the cross-sectional area along which the profile density is calculated, as well as an optional filter to remove lower density values (useful for MXD studies). Automatic batch calculation of density profiles with different settings afterward is also an option. The program can handle missing rings, and fractures in a core that should not be included in the density profile. There is also an option to display an average of multiple slices that accounts for the orientation of the ring borders. This is particularly useful when handling extremely narrow rings or very noisy scans. All indication data and density profiles are saved as *.txt* files, that accompany the digital core.

5.3. CoreComparison and XCT.read R function

CoreComparison facilitates cross-dating by displaying ring-width curves of indicated cores and optional reference chronologies. When changes are made in *RingIndicator*, such as adjusting indications or the felling date, these updates will be reflected in *CoreComparison* by pressing the refresh button. It also calculates inter-series gleichläufigkeit (GLK) (Eckstein and Bauch, 1969; Buras and Wilmking, 2015) and correlation statistics between all loaded series.

The *XCT.read* R function (R Core Team, 2024) was created to easily read and calculate ring width and density parameters using the txt-formatted ring indications and density profile output from

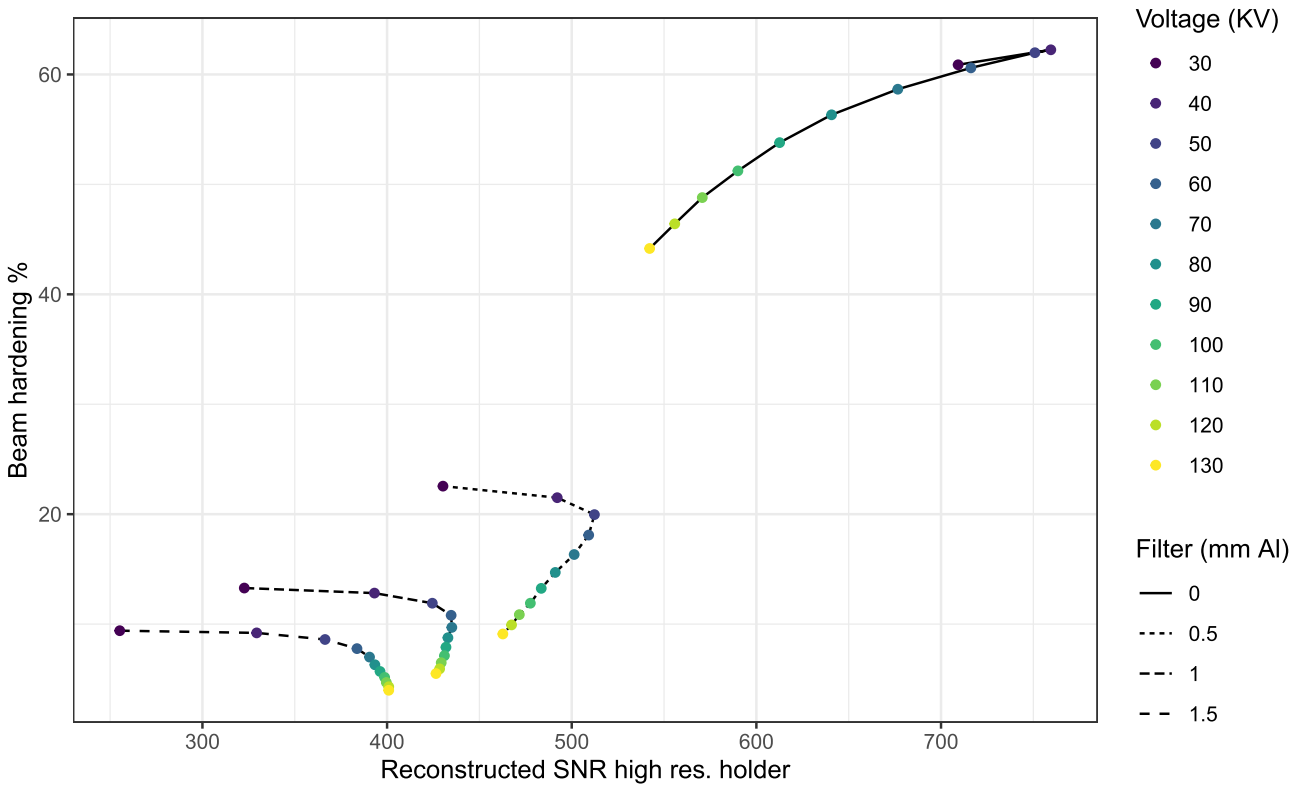

Fig. A.1. Arion simulation of the high-resolution holder. It shows the expected beam hardening and signal-to-noise ratio in the reconstruction. Different combinations of voltage and aluminum filter thickness are shown.

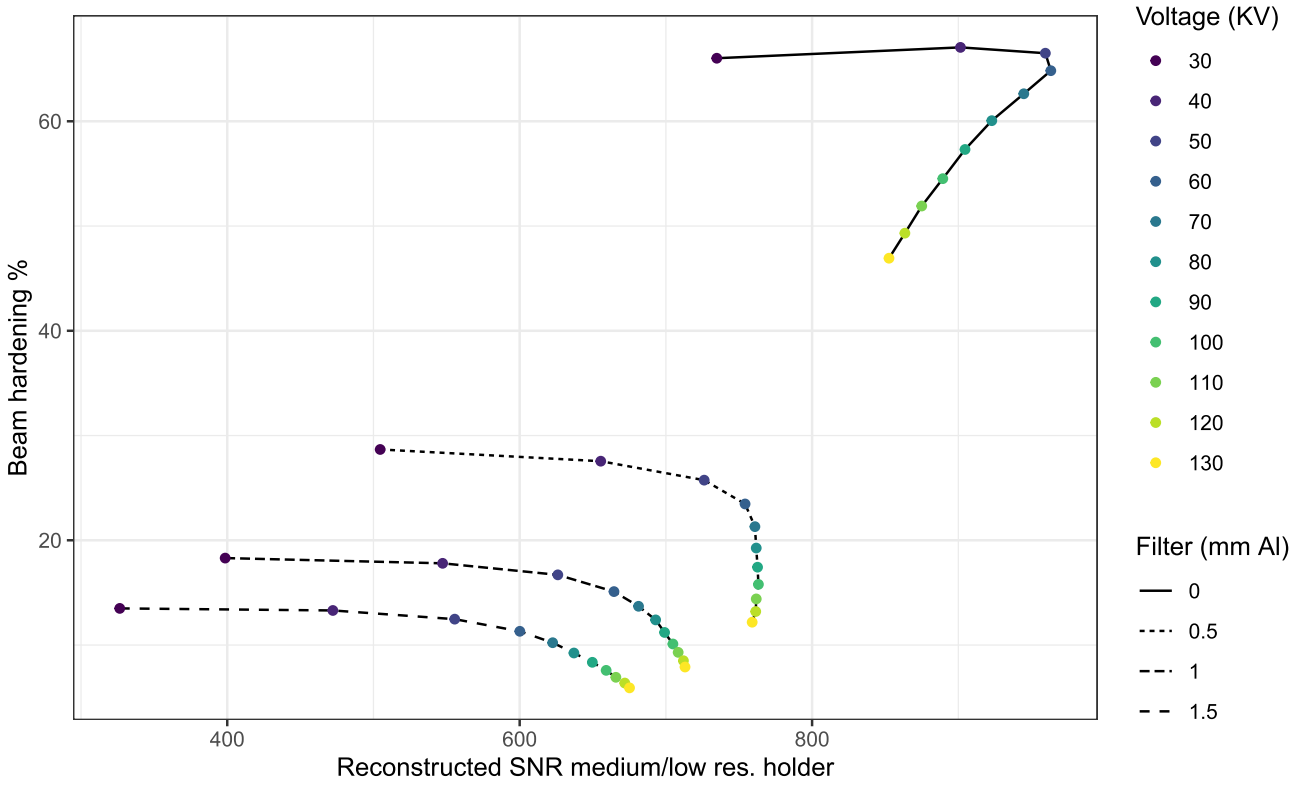

Fig. A.2. Arion simulation of the medium/low-resolution holder. It shows the expected beam hardening and signal-to-noise ratio in the reconstruction. Different combinations of voltage and aluminum filter thickness are shown.

Table B.1
An overview of the reference samples, their gravimetric density, and the average error for each species in each of the 4 scan modes. All shown results are the average of three replicates. *Picea abies* is represented by six samples: three with wide rings (5 mm) and three with narrow rings (0.5 mm). *Pinus rigida* is also represented by six samples, three that were treated by water and ethanol Soxhlet extraction, and three that were not extracted. All other samples have not been Soxhlet extracted. The species are ordered from low to high density.

Species	Gravimetric density (g/cm^3)	High res. fast (g/cm^3)	High res. optimal (g/cm^3)	Medium res. (g/cm^3)	Low res. (g/cm^3)	Average error (g/cm^3)
***Ochroma pyramidale* Urb.**	0.110	−0.001	−0.001	−0.004	+ 0.000	−0.002
***Picea abies* (L.) H. Karst. fast growth**	0.403	−0.008	−0.006	−0.003	+ 0.000	−0.004
***Populus x canadensis* Moench**	0.459	−0.008	−0.006	+ 0.003	+ 0.000	−0.003
***Picea abies* (L.) H. Karst. slow growth**	0.524	−0.008	−0.004	+ 0.006	+ 0.011	+ 0.001
***Tillia cordata* Mill.**	0.582	−0.008	−0.006	+ 0.012	+ 0.007	+ 0.001
***Pseudotsuga menziesii* (Mirbel) Franco**	0.583	−0.020	−0.017	−0.002	−0.004	−0.011
***Betula pendula* Roth**	0.586	−0.010	−0.009	+ 0.011	+ 0.006	+ 0.000
***Quercus robur* L.**	0.601	−0.025	−0.022	−0.005	−0.008	−0.015
***Fagus sylvatica* L.**	0.697	−0.009	−0.006	+ 0.015	+ 0.009	+ 0.002
***Afzelia bipindensis* Harms**	0.716	+ 0.038	+ 0.041	+ 0.053	+ 0.052	+ 0.046
***Pinus rigida* Mill. soxhlet**	0.746	+ 0.007	+ 0.012	+ 0.031	+ 0.031	+ 0.020
***Pinus rigida* Mill. no soxhlet**	0.779	−0.026	−0.022	+ 0.006	+ 0.004	−0.010
Handroanthus spp.	0.905	−0.022	−0.018	+ 0.003	+ 0.000	−0.009
***Lophira alata* Banks**	1.059	−0.029	−0.027	+ 0.004	+ 0.003	−0.012

RingIndicator. The section of the profile where a density parameter is calculated can be set by the user: either a fraction of the ring (e.g. the second quarter of each ring) or a fixed width (e.g. the last 100 μm of each ring). The output of the function is a *dplR* (Bunn, 2008) or a long format data frame.

6. Human labor time

Minimizing human labor time is critical for the scalability of tree-ring densitometry studies. Accordingly, the workflow detailed in this paper has been systematically optimized to reduce manual intervention and enhance operational efficiency. Table 3 provides a comparative overview of the labor hours required for high- and medium/low-resolution scans. The times presented encompass all steps resulting in a digital image that is ready for ring indications. Since the labor time needed for ring boundary indication is highly sample-dependent and has significant automation potential, it is excluded from this overview.

Table 3 demonstrates that the XμCT method is highly labor-efficient, only requiring a total of approximately 2.2 min per 35 cm of medium/low-resolution sample and 5.4 min per 35 cm of high-resolution sample. This is orders of magnitude faster than the conventional DENDRO2003 - WALESCH Electronic approach (Lenz et al., 1976; Schweingruber et al., 1978; Evans, 1994), and is comparable to optical blue intensity (McCarroll et al., 2002; Campbell et al., 2007; Rydval et al., 2014) in this regard. This is thanks to the digital nature of the XμCT workflow and the minimal manual operations required for each core. Efficiency is further boosted by the large batch sizes and long core lengths facilitated by the sample holders, reducing the number of scans needed per study. Note that conifer MXD studies require a Soxhlet extraction to remove resins. This adds approximately 2–3 min of labor time per sample when using the current setup at our lab. This could however be further optimized in the future.

7. Reference samples

A set of reference samples with a known density was created to check if our XμCT-densities are comparable with gravimetric density measurements. They were used to detect errors in hardware and software, directly compare between different scan settings, identify the accuracy and limitations of the XμCT approach, and can be used to compare different scanners in the future. The 42 reference samples are 6 mm diameter cylinders, 7 cm in length, and cover a wide range of low to high-density conifers and broadleaved temperate and tropical species, with narrow to wide rings. Each species is represented by 3 samples. An overview of the selected species can be found in Figure 4. The gravimetric density was determined by weighing the oven-dry mass and determining the exact oven-dry volume from 30 μm XμCT scans. the XμCT-based volume is more accurate than the Archimedes-based volume in this case due to the small size and large surface area of these increment core-like samples. The samples were subsequently scanned in the four scanning modes (see Table 1). The average XμCT density could then be compared with the gravimetric density. The results are presented in Figure 4 and Table B.1.

Overall, the XμCT density showed an average error of −0.0004 g/cm^3 or −0.06 %. This differs slightly between scan modes and depends on the species. The high-resolution fast and high-resolution optimal scan modes underestimated the density by −0.009 g/cm^3 and −0.007 g/cm^3 or −1.4 % and −1.1 % respectively, while medium and low-resolution scan modes overestimated density by + 0.009 g/cm^3 and + 0.008 g/cm^3 or + 1.1 % and + 1.1 %. Most species show small overall errors with 11 of the 14 species having an absolute error below 2 %. The largest biases are found in *Afzelia bipindensis* with an average error of + 0.046 g/cm^3 or 6.44 %, which can probably be attributed to crystals or crystal-like structures. Diffraction caused by crystals can cause an overestimation of wood density when using X-ray-based techniques (Vansteenkiste et al., 2007; Polge, 1966). Caution is thus advised when using XμCT for wood density studies on species with high amounts of crystals or crystal-like structures.

8. Limitations and solutions

The primary limitation of this pipeline is the required infrastructure. XμCT scanners, such as the CoreTOM, are costly and require specialized staff for operation and maintenance. Additionally, achieving optimal results necessitates a XμCT system with a high-pixel-density detector and preferably a slow and stable vertical axis, which further increases the complexity and expense of the setup. However, many countries host research facilities dedicated to XμCT, such as NXCT in the UK, UTCT in Texas, INRS lab CT scan in Canada, and UGCT in Belgium. These facilities are designed to mitigate this infrastructure limitation and promote the widespread use of XμCT across various scientific fields. The presented toolchain was developed at the UGent-Woodlab and UGCT (UGent Center for X-ray Tomography) and we welcome any international collaborators interested in applying XμCT-based tree-ring densitometry in their research.

Working with XμCT images often necessitates PCs with substantial amounts of RAM. The new versions of the software partially address this by eliminating the need to load entire scans at once. Nonetheless, a minimum of 64 GB of RAM is recommended, which is sufficient to handle the largest samples produced by the presented setup.

Measuring the density of species with high amounts of crystals or crystal-like structures (often in the tropics) with X-ray-based techniques is a challenge, as evidenced by the reference scan of *Afzelia*. These components do not adhere to the attenuation-density relationship as determined through the air-POM referencing, resulting in incorrect density measurements. A potential solution could be to attempt chemical extraction of these components (Sheppard and Thompson, 2000; Scharnweber et al., 2023).

All XμCT images inherently exhibit some degree of artifacts, regardless of the object or scanner. Currently, we are contending with an artifact that, in specific cases, can inaccurately represent a tree-ring boundary. This artifact predominantly affects samples with extremely narrow rings (e.g. slow-growing bristlecone pine (De Mil et al., 2024)). In those cases, this artifact results in approximately 5 % of the rings that can't be used for density measurements. Additionally, in such samples the 15 μm resolution may be insufficient, as some ring widths approach the 30–60 μm limit, to be able to resolve the ring at all. However, the use of measuring X-ray density-based MXD in rings that are only a few cells wide might be questionable. While scanning at higher resolution, e.g. 7.5 μm, is possible, it is not recommended due to the higher noise levels, extended scan times, exponentially larger data sizes (approximately 45 GB per 35 cm sample), and reduced sample throughput (only four to five samples per scan). Moreover, at such resolutions, individual tracheids start to become visible. Therefore, in such extreme cases, it makes more sense to do an anatomical analysis on, for example, cross-sections (Yasue et al., 2000; Decoux et al., 2004; von Arx et al., 2016; Björklund et al., 2019,2020). XμCT can also be used for that purpose (Van den Bulcke et al., 2019), but no high-throughput protocols have been designed so far to overcome the large scan time and data volumes.

9. Discussion, outlook, and conclusions

The X-ray micro-CT pipeline described in this paper represents a significant advancement in the field of tree-ring densitometry and is the result of more than 10 years of development at UGent-Woodlab and UGCT. The presented workflow can process large amounts of samples in a limited timeframe. This is crucial for large-scale studies, facilitating the analysis of extensive datasets with higher efficiency. These datasets not only advance our understanding of historical climate conditions but are also invaluable for modeling carbon stocks. Optimization and standardization of the scanning process ensure consistent and high-quality data acquisition, which can potentially be applied at other XμCT scanning facilities. This uniformity would enable fully inter-comparable datasets, thereby enhancing collaborative research efforts.

Blue intensity emerged a few decades ago as a rapid and cost-effective alternative to X-ray densitometry (McCarroll et al., 2002; Campbell et al., 2007; Rydval et al., 2014). The protocol presented here demonstrates that XμCT densitometry can achieve comparable speed and affordability while offering the advantages of direct density measurements, free from issues such as wood discoloration and light intensity biases (Rydval et al., 2014; Bjorklund et al., 2014; Wilson et al., 2017; Björklund et al., 2019, 2021; Seftigen et al., 2020; Wang et al., 2020). Although anatomical approaches in dendroclimatology (Yasue et al., 2000; von Arx et al., 2016; Rydval et al., 2024) are probably superior to integrated wood density measurements due to resolution effects (Decoux et al., 2004; Björklund et al., 2019,2020; Seftigen et al., 2022; Björklund et al., 2023), they are highly labor-intensive. In contrast, the proposed XμCT pipeline offers a densitometry technique with a much lower demand for human labor. As such, this XμCT approach might be the optimal density-related measuring technique for large-scale tree-ring densitometry studies in terms of striking a balance between speed, cost, and quality. Furthermore, as a non-destructive method, XμCT opens new avenues for multi-proxy datasets. After measuring density and ring width with XμCT, samples remain available for further analysis, such as laser ablation isotope analysis (Loader et al., 2017), optical imaging (Rydval et al., 2024; Van den Bulcke et al., 2025), or anatomical analysis on cross-sections (Yasue et al., 2000; von Arx et al., 2016).

An alternative workflow, optimized for large-scale carbon stock studies involving tens of thousands of samples, has already been developed using medical CT scanners (Jacquin et al., 2019; Cuny et al., 2024). This approach is tailored for applications that do not require tree-ring analysis or corrections for fiber and ring angles. It utilizes very low-resolution scans (300–600 μm) and large sample holders to efficiently process these extensive collections. Similarly, our methodology could be adapted to such studies by designing a new high-capacity sample holder, capable of accommodating hundreds of samples per scan, thereby further enhancing our throughput to facilitate these types of studies.

The digital copy of increment cores created with XμCT enables interesting image processing possibilities. For instance, Martinez-Garcia et al. (2021) utilized X-ray computed tomography data to generate 3D representations of tree-ring boundaries. The digital 3D density data produced by our pipeline is particularly well-suited for deep learning applications, such as the detection and segmentation of individual tree rings. Integrating these techniques could further accelerate large-scale tree-ring densitometry studies. Consequently, future work should focus on incorporating deep learning-based automatic tree-ring detection into the existing toolchain and exploring density parameters based on 3D ring segmentations.

In summary, the pipeline detailed in this paper sets the stage for significant progress in tree-ring densitometry research and its applications in climate science and ecology. The combination of efficient hardware, optimized workflows, and advanced software tools creates a powerful platform for future research.

CRediT authorship contribution statement

Charlotte Pearson: Writing – review & editing, Funding acquisition. **Jorden De Bolle:** Writing – review & editing, Methodology. **Tom De Mil:** Writing – review & editing, Funding acquisition. **Valerie Trouet:** Writing – review & editing, Funding acquisition. **Louis Verschuren:** Writing – review & editing, Writing – original draft, Visualization, Software, Methodology, Investigation, Formal analysis, Data curation, Conceptualization. **Vladimir Matskovsky:** Writing – review & editing, Visualization, Validation, Software, Methodology, Conceptualization. **Toon Gheyle:** Writing – review & editing, Methodology. **Jan Van den Bulcke:** Writing – review & editing, Visualization, Validation, Supervision, Resources, Project administration, Methodology, Funding acquisition, Conceptualization. **Joris Van Acker:** Writing – review & editing, Supervision. **Matthieu N. Boone:** Writing – review & editing, Methodology. **Luc Van Hoorebeke:** Writing – review & editing, Funding acquisition.

Declaration of Competing Interest

The authors declare that they have no known competing financial interests or personal relationships that could have appeared to influence the work reported in this paper.

Data availability

The latest versions of the software packages, comprehensive video manuals, test datasets, heel correction code, and CAD drawings of the holders are all freely available at https://dendrochronomics.ugent.be with backups on Zenodo: https://doi.org/10.5281/zenodo.14677732 (compiled MATLAB packages and Excel templates), https://doi.org/10.5281/zenodo.14654939 (XCT.Read R function and examples), https://doi.org/10.5281/zenodo.14653186 (Sample holder STL files, Data and code for the reference sample figure), https://doi.org/10.5281/zenodo.14824998 (sample scans and increment core volumes). Larger sample scans are available on request.

Acknowledgements

We acknowledge financial support from the Special Research Fund (BOF) for the UGCT Core Facility (BOF.COR.2022.008), the IOF for project FaCT F2021/IOF-Equip/021, and the Research Foundation—Flanders (FWO) for the ACTREAL (G019521N) and XyloDynaCT (G00972ON) projects. We would like to thank Pierre Kibleur for the help with Arion. We are grateful to Stijn Willen, Yves Israel, Pieter Tack, Iván Josipovic, and Rudi Hoeben for technical and IT support.

References under review

De Bolle J., Verschuren L., Van den Bulcke J., Boone M.N. Correction for the heel effect in helical μCT scans for accurate densitometry. Precision Engineering. [Under Review].

Appendix A. Arion simulations

A 100 kV beam with a 0.5 mm aluminum (Al) filter was selected to strike a balance between minimizing beam hardening and maximizing the signal-to-noise ratio (SNR). While a 1 mm Al filter effectively reduces beam hardening, it significantly compromises SNR. Conversely, using no filter (0 mm) can lead to notable errors even after beam hardening correction and heeling correction, as second-order effects like pitting may still introduce inaccuracies.

Fig. A.1

Fig. A.2

B. Reference samples

Table B.1

References

Babst, F., Bouriaud, O., Poulter, B., Trouet, V., Girardin, M.P., Frank, D.C., 2019. Twentieth century redistribution in climatic drivers of global tree growth. Sci. Adv. 5, eaat4313. https://doi.org/10.1126/sciadv.aat4313.

Bjorklund, J., Gunnarson, B., Seftigen, K., Esper, J., Linderholm, H., 2014. Blue intensity and density from northern fennoscandian tree rings, exploring the potential to improve summer temperature reconstructions with earlywood information. Climate 10, 877–885. https://doi.org/10.5194/cp-10-877-2014.

Björklund, J., Seftigen, K., Schweingruber, F., Fonti, P., von Arx, G., Bryukhanova, M.V., Cuny, H.E., Carrer, M., Castagneri, D., Frank, D.C., 2017. Cell size and wall dimensions drive distinct variability of earlywood and latewood density in northern hemisphere conifers. N. Phytol. 216, 728–740. https://doi.org/10.1111/nph.14639.

Björklund, J., von Arx, G., Nievergelt, D., Wilson, R., Van den Bulcke, J., Günther, B., Loader, N.J., Rydval, M., Fonti, P., Scharnweber, T., Andreu-Hayles, L., Büntgen, U., D'Arrigo, R., Davi, N., De Mil, T., Esper, J., Gärtner, H., Geary, J., Gunnarson, B.E., Hartl, C., Hevia, A., Song, H., Janecka, K., Kaczka, R.J., Kirdyanov, A.V., Kochbeck, M., Liu, Y., Meko, M., Mundo, I., Nicolussi, K., Oelkers, R., Pichler, T., Sánchez-Salguero, R., Schneider, L., Schweingruber, F., Timonen, M., Trouet, V., Van Acker, J., Verstege, A., Villalba, R., Wilmking, M., Frank, D., 2019. Scientific merits and analytical challenges of tree-ring densitometry. Rev. Geophys. 57, 1224–1264. https://doi.org/10.1029/2019RG000642.

Björklund, J., Seftigen, K., Fonti, P., Nievergelt, D., von Arx, G., 2020. Dendroclimatic potential of dendroanatomy in temperature-sensitive Pinus sylvestris. Dendrochronologia 60, 125673. https://doi.org/10.1016/j.dendro.2020.125673.

Björklund, J., von Arx, G., Fonti, P., Stridbeck, P., De Mil, T., Neycken, A., Seftigen, K., 2021. The utility of bulk wood density for tree-ring research. Dendrochronologia 69, 125880. https://doi.org/10.1016/j.dendro.2021.125880.

Björklund, J., Seftigen, K., Stoffel, M., Fonti, M.V., Kottlow, S., Frank, D.C., Esper, J., Fonti, P., Goosse, H., Grudd, H., Gunnarson, B.E., Nievergelt, D., Pellizzari, E., Carrer, M., von Arx, G., 2023. Fennoscandian tree-ring anatomy shows a warmer modern than medieval climate. Nature 620, 97–103. https://doi.org/10.1038/s41586-023-06176-4.

Braun, H., Kyriakou, Y., Kachelrieß, M., Kalender, W.A., 2010. The influence of the heel effect in cone-beam computed tomography: artifacts in standard and novel geometries and their correction. Phys. Med. Biol. 55, 6005. https://doi.org/10.1088/0031-9155/55/19/024.

Briffa, K., Osborn, T., Schweingruber, F., 2004. Large-scale temperature inferences from tree rings: a review. Glob. Planet. Change 40, 11–26. https://doi.org/10.1016/S0921-8181(03)00095-X.

Briffa, K.R., 1999. Interpreting high-resolution proxy climate data — the example of dendroclimatology. In: vonStorch, H., Navarra, A. (Eds.), Analysis of Climate Variability, Springer Berlin Heidelberg, Berlin, Heidelberg, pp. 77–94. https://doi.org/10.1007/978-3-662-03744-7_5.

Bunn, A.G., 2008. A dendrochronology program library in r (dplr). Dendrochronologia 26, 115–124. https://doi.org/10.1016/j.dendro.2008.01.002.

Büntgen, U., Esper, J., 2024. The need for high-resolution paleoclimate research, 29768659241305959 Dialog-. Clim. Change 0. https://doi.org/10.1177/29768659241305959.

Buras, A., Wilmking, M., 2015. Correcting the calculation of gleichläufigkeit. Dendrochronologia 34, 29–30. https://doi.org/10.1016/j.dendro.2015.03.003.

Campbell, R., McCarroll, D., Loader, N.J., Grudd, H., Robertson, I., Jalkanen, R., 2007. Blue intensity in Pinus sylvestris tree-rings: developing a new palaeoclimate proxy. Holocene 17, 821–828. https://doi.org/10.1177/0959683607080523.

Chave, J., Réjou-Méchain, M., Búrquez, A., Chidumayo, E., Colgan, M.S., Delitti, W.B., Duque, A., Eid, T., Fearnside, P.M., Goodman, R.C., Henry, M., Martínez-Yrízar, A., Mugasha, W.A., Muller-Landau, H.C., Mencuccini, M., Nelson, B.W., Ngomanda, A., Nogueira, E.M., Ortiz-Malavassi, E., Pélissier, R., Ploton, P., Ryan, C.M., Saldarriaga, J.G., Vieilledent, G., 2014. Improved allometric models to estimate the aboveground biomass of tropical trees. Glob. Change Biol. 20, 3177–3190. https://doi.org/10.1111/gcb.12629.

Cuny, H., Leban, J.M., Hervé, A., et al., 2024.XyloDensMap: an intensive georeferenced data record for the wood density of European trees.Research Square 10.21203/rs.3.rs-5432732/v1. preprint (Version 1).

De Mil, T., Van den Bulcke, J., 2023. Tree core analysis with x-ray computed tomography. JoVE, e65208. https://doi.org/10.3791/65208.

De Mil, T., Vannoppen, A., Beeckman, H., Van Acker, J., Van den Bulcke, J., 2016. A field-to-desktop toolchain for x-ray ct densitometry enables tree ring analysis. Ann. Bot. 117, mcw063. https://doi.org/10.1093/aob/mcw063.

De Mil, T., Matskovsky, V., Salzer, M., Corluy, L., Verschuren, L., Pearson, C., Van Hoorebeke, L., Trouet, V., Van den Bulcke, J., 2024. Bristlecone pine maximum latewood density as a superior proxy for millennium-length temperature reconstructions. Geophys. Res. Lett., e2024GL109799 https://doi.org/10.1029/2024GL109799 e2024GL109799 2024GL109799.

De Ridder, M., Van den Bulcke, J., Vansteenkiste, D., Van Loo, D., Dierick, M., Masschaele, B., De Witte, Y., Mannes, D., Lehmann, E., Beeckman, H., Van Hoorebeke, L., Van Acker, J., 2011. High-resolution proxies for wood density variations in Terminalia superba. Ann. Bot. 107, 293–302. https://doi.org/10.1093/aob/mcq224.

De Witte, Y., 2010.Improved and practically feasible reconstruction methods for high resolution X-ray tomography.Ph.D. thesis.Ghent University.

Decoux, V., Varcin, É ., Leban, J.M., 2004. Relationships between the intra-ring wood density assessed by x-ray densitometry and optical anatomical measurements in conifers. consequences for the cell wall apparent density determination. Ann. For. Sci. 61, 251–262. https://doi.org/10.1051/forest:2004018.

Dhaene, J., Pauwels, E., De Schryver, T., De Muynck, A., Dierick, M., Van Hoorebeke, L., 2015. A realistic projection simulator for laboratory based x-ray micro-ct. Nucl. Instrum. Methods Phys. Res. Sect. B: Beam Interact. Mater. At. 342, 170–178. https://doi.org/10.1016/j.nimb.2014.09.033.

Dierick, M., Masschaele, B., Hoorebeke, L.V., 2004. Octopus, a fast and user-friendly tomographic reconstruction package developed in LabView®. Meas. Sci. Technol. 15, 1366–1370. https://doi.org/10.1088/0957-0233/15/7/020.

Eckstein, D., Bauch, J., 1969. Beitrag zur rationalisierung eines dendrochronologischen verfahrens und zur analyse seiner aussagesicherheit. Forstwiss. Cent. 88, 230–250. https://doi.org/10.1007/BF02741777.

Esper, J., Frank, D.C., Timonen, M., Zorita, E., Wilson, R.J.S., Luterbacher, J., Holzkämper, S., Fischer, N., Wagner, S., Nievergelt, D., Verstege, A., Büntgen, U., 2012. Orbital forcing of tree-ring data. Nat. Clim. Change 2, 862–866. https://doi.org/10.1038/nclimate1589.

Evans, R., 1994. Rapid measurement of the transverse dimensions of tracheids in radial wood sections from Pinus radiata. Holzforschung 48, 168–172. https://doi.org/10.1515/hfsg.1994.48.2.168.

Fodor, F., 1999. The densest packing of 19 congruent circles in a circle. Geom. Dedicata 74, 139–145. https://doi.org/10.1023/A:1005091317243.

Hubau, W., De Mil, T., Van den Bulcke, J., Phillips, O.L., Angoboy Ilondea, B., Van Acker, J., Sullivan, M.J.P., Nsenga, L., Toirambe, B., Couralet, C., Banin, L.F., Begne, S.K., Baker, T.R., Bourland, N., Chezeaux, E., Clark, C.J., Collins, M., Comiskey, J.A., Cuni-Sanchez, A., Deklerck, V., Dierickx, S., Doucet, J.L., Ewango, C. E.N., Feldpausch, T.R., Gilpin, M., Gonmadje, C., Hall, J.S., Harris, D.J., Hardy, O.J., Kamdem, M.N.D., KasongoYakusu, E., Lopez-Gonzalez, G., Makana, J.R., Malhi, Y., Mbayu, F.M., Moore, S., Mukinzi, J., Pickavance, G., Poulsen, J.R., Reitsma, J., Rousseau, M., Sonké, B., Sunderland, T., Taedoumg, H., Talbot, J., Tshibamba Mukendi, J., Umunay, P.M., Vleminckx, J., White, L.J.T., Zemagho, L., Lewis, S.L., Beeckman, H., 2019. The persistence of carbon in the african forest understory. Nat. Plants 5, 133–140. https://doi.org/10.1038/s41477-018-0316-5.

Jacquin, P., Longuetaud, F., Leban, J.M., Mothe, F., 2017. X-ray microdensitometry of wood: A review of existing principles and devices. Dendrochronologia 42, 42–50. https://doi.org/10.1016/j.dendro.2017.01.004.

Jacquin, P., Mothe, F., Longuetaud, F., Billard, A., Kerfriden, B., Leban, J.M., 2019. Carden: a software for fast measurement of wood density on increment cores by ct scanning. Comput. Electron. Agric. 156, 606–617. https://doi.org/10.1016/j.compag.2018.12.008. ⟨https://www.sciencedirect.com/science/article/pii/S0168169918313255⟩.

Jones, P., Briffa, K., Osborn, T., Lough, J., van Ommen, T., Vinther, B., Luterbacher, J., Wahl, E., Zwiers, F., Mann, M., Schmidt, G., Ammann, C., Buckley, B., Cobb, K., Esper, J., Goosse, H., Graham, N., Jansen, E., Kiefer, T., Kull, C., Küttel, M., Mosley-Thompson, E., Overpeck, J., Riedwyl, N., Schulz, M., Tudhope, A., Villalba, R., Wanner, H., Wolff, E., Xoplaki, E., 2009. High-resolution palaeoclimatology of the last millennium: a review of current status and future prospects. Holocene 19, 3–49. https://doi.org/10.1177/0959683608098952.

Katsevich, A., 2002. Theoretically exact filtered backprojection-type inversion algorithm for spiral ct. SIAM J. Appl. Math. 62, 2012–2026. https://doi.org/10.1137/S0036139901387186.

Lenz, O., Schär, E., Schweingruber, F.H., 1976. Methodische probleme bei der radiographisch-densitometrischen bestimmung der dichte und der jahrringbreiten von holz. Holzforschung 30, 114–123. https://doi.org/10.1515/hfsg.1976.30.4.114.

Loader, N., McCarroll, D., Barker, S., Jalkanen, R., Grudd, H., 2017. Inter-annual carbon isotope analysis of tree-rings by laser ablation. Chem. Geol. 466, 323–326. https://doi.org/10.1016/j.chemgeo.2017.06.021.

Lubachevsky, B.D., Graham, R.L., 1997. Curved hexagonal packings of equal disks in a circle. Discret. Comput. Geom. 18, 179–194. https://doi.org/10.1007/PL00009314.

Martinez-Garcia, J., Stelzner, I., Stelzner, J., Gwerder, D., Schuetz, P., 2021. Automated 3d tree-ring detection and measurement from x-ray computed tomography. Dendrochronologia 69, 125877. https://doi.org/10.1016/j.dendro.2021.125877.

McCarroll, D., Pettigrew, E., Luckmana, A., Guibal, F., Edouard, J.L., 2002. Blue reflectance provides a surrogate for latewood density of high-latitude pine tree rings. Arct., Antarct., Alp. Res. 34, 450–453. https://doi.org/10.1080/15230430.2002.12003516.

Moonen, P., Dhaene, J., Van den Bulcke, J., Boone, M.N., Van Hoorebeke, L., 2022. Calibration-free retrieval of density information from computed tomography data. Precis. Eng. 76, 377–384. https://doi.org/10.1016/j.precisioneng.2022.04.001.

Pennefather, P.S., Suhanic, W., 2009. Biotiff: a new bigtiff file structure for organizing large image datasets and their associated metadata. Biophys. J. 96, 30a. https://doi.org/10.1016/j.bpj.2008.12.045.

Polge, H., 1966.Établissement des courbes de variation de la densité du bois par exploration densitométrique de radiographies d'échantillons prélevés à la tarière sur des arbres vivants: applications dans les domaines technologique et physiologique, in: Annales des sciences forestières, EDP Sciences.I-206.

R Core Team, 2024.R: A Language and Environment for Statistical Computing. R Foundation for Statistical Computing. Vienna, Austria.⟨https://www.R-project.org/⟩.

Rydval, M., Åke Larsson, L., McGlynn, L., Gunnarson, B.E., Loader, N.J., Young, G.H., Wilson, R., 2014. Blue intensity for dendroclimatology: should we have the blues? experiments from scotland. Dendrochronologia 32, 191–204. https://doi.org/10.1016/j.dendro.2014.04.003.

Rydval, M., Björklund, J., von Arx, G., Begović, K., Lexa, M., Nogueira, J., Schurman, J. S., Jiang, Y., 2024. Ultra-high-resolution reflected-light imaging for dendrochronology. Dendrochronologia 83, 126160. https://doi.org/10.1016/j.dendro.2023.126160.

Scharnweber, T., Rocha, E., González Arrojo, A., Ahlgrimm, S., Gunnarson, B.E., Holzkämper, S., Wilmking, M., 2023. To extract or not to extract? influence of chemical extraction treatment of wood samples on element concentrations in tree-rings measured by x-ray fluorescence. Front. Environ. Sci. 11. https://doi.org/10.3389/fenvs.2023.1031770.

Schindelin, J., Arganda-Carreras, I., Frise, E., Kaynig, V., Longair, M., Pietzsch, T., Preibisch, S., Rueden, C., Saalfeld, S., Schmid, B., Tinevez, J.Y., White, D.J., Hartenstein, V., Eliceiri, K., Tomancak, P., Cardona, A., 2012. Fiji: an open-source platform for biological-image analysis. Nat. Methods 9, 676–682. https://doi.org/10.1038/nmeth.2019.

Schweingruber, F.H., Fritts, H.C., Bräker, O.U., Drew, L.G., Schär, E., 1978.The x-ray technique as applied to dendroclimatology.Tree-Ring Bulletin ⟨http://hdl.handle.net/10150/260420⟩.

Seftigen, K., Fuentes, M., Ljungqvist, F.C., Björklund, J., 2020. Using blue intensity from drought-sensitive Pinus sylvestris in fennoscandia to improve reconstruction of past hydroclimate variability. Clim. Dyn. 55, 579–594. https://doi.org/10.1007/s00382-020-05287-2.

Seftigen, K., Fonti, M.V., Luckman, B., Rydval, M., Stridbeck, P., von Arx, G., Wilson, R., Björklund, J., 2022. Prospects for dendroanatomy in paleoclimatology – a case study on Picea engelmannii from the canadian rockies. Climate 18, 1151–1168. https://doi.org/10.5194/cp-18-1151-2022.

Sheppard, P.R., Thompson, T.L., 2000. Effect of extraction pretreatment on radial variation of nitrogen concentration in tree rings. J. Environ. Qual. 29, 2037–2042. https://doi.org/10.2134/jeq2000.00472425002900060042x.

Swetnam, T.W., Allen, C.D., Betancourt, J.L., 1999. Applied historical ecology: Using the past to manage for the future. Ecol. Appl. 9, 1189–1206. https://doi.org/10.1890/1051-0761(1999)009[1189:AHEUTP]2.0.CO;2.

The MathWorks Inc., 2024. Matlab version: R2024b. Natick, Massachusetts, United States. ⟨https://www.mathworks.com⟩.

Van den Bulcke, J., Wernersson, E.L., Dierick, M., Van Loo, D., Masschaele, B., Brabant, L., Boone, M.N., Van Hoorebeke, L., Haneca, K., Brun, A., Luengo Hendriks, C.L., Van Acker, J., 2014. 3d tree-ring analysis using helical x-ray tomography. Dendrochronologia 32, 39–46. https://doi.org/10.1016/j.dendro.2013.07.001.

Van den Bulcke, J., Boone, M., Dhaene, J., Denis, V., Hoorebeke, L., Boone, M., Wyffels, F., Beeckman, H., Van Acker, J., De Mil, T., 2019. Advanced x-ray ct scanning can boost tree-ring research for earth-system sciences. Ann. Bot. 124, 837–847. https://doi.org/10.1093/aob/mcz126.

Van den Bulcke, J., Verschuren, L., De Blaere, R., Vansuyt, S., Dekegeleer, M., Kibleur, P., Pieters, O., De Mil, T., Hubau, W., Beeckman, H., Van Acker, J., wyffels, F., 2025. Enabling high-throughput quantitative wood anatomy through a dedicated pipeline. Plant Methods 21, 11. https://doi.org/10.1186/s13007-025-01330-7.

Vannoppen, A., Maes, S., Kint, V., De Mil, T., Ponette, Q., Van Acker, J., Van den Bulcke, J., Verheyen, K., Muys, B., 2017. Using x-ray ct based tree-ring width data for tree growth trend analysis. Dendrochronologia 44, 66–75. https://doi.org/10.1016/j.dendro.2017.03.003.

Vannoppen, A., Boeckx, P., De Mil, T., Kint, V., Ponette, Q., Van den Bulcke, J., Verheyen, K., Muys, B., 2018. Climate driven trends in tree biomass increment show asynchronous dependence on tree-ring width and wood density variation. Dendrochronologia 48, 40–51. https://doi.org/10.1016/j.dendro.2018.02.001.

Vansteenkiste, D., Van Acker, J., Stevens, M., LeThiec, D., Nepveu, G., 2007. Composition, distribution and supposed origin of mineral inclusions in sessile oak wood — consequences for microdensitometrical analysis. Ann. For. Sci. 64, 11–19. https://doi.org/10.1051/forest:2006083.

Vlassenbroeck, J., Dierick, M., Masschaele, B., Cnudde, V., Van Hoorebeke, L., Jacobs, P., 2007. Software tools for quantification of x-ray microtomography at the ugct. Nucl. Instrum. Methods Phys. Res. Sect. A: Accel., Spectrometers, Detect. Assoc. Equip. 580, 442–445. https://doi.org/10.1016/j.nima.2007.05.073 proceedings of the 10 th International Symposium on Radiation Physics.

von Arx, G., Crivellaro, A., Prendin, A.L., Čufar, K., Carrer, M., 2016. Quantitative wood anatomy–practical guidelines. Front. Plant Sci. 7. https://doi.org/10.3389/fpls.2016.00781.

Wang, F., Arseneault, D., Boucher, E., Yu, S., Ouellet, S., Chaillou, G., Delwaide, A., Wang, L., 2020. Chemical destaining and the delta correction for blue intensity measurements of stained lake subfossil trees. Biogeosciences 17, 4559–4570. https://doi.org/10.5194/bg-17-4559-2020.

Wilson, R., Luckman, B., 2003. Dendroclimatic reconstruction of maximum summer temperatures from upper treeline sites in interior british columbia, canada. Holocene 136, 851–861. https://doi.org/10.1191/0959683603hl663rp.

Wilson, R., Anchukaitis, K., Briffa, K.R., Büntgen, U., Cook, E., D'Arrigo, R., Davi, N., Esper, J., Frank, D., Gunnarson, B., Hegerl, G., Helama, S., Klesse, S., Krusic, P.J., Linderholm, H.W., Myglan, V., Osborn, T.J., Rydval, M., Schneider, L., Schurer, A., Wiles, G., Zhang, P., Zorita, E., 2016. Last millennium northern hemisphere summer temperatures from tree rings: Part i: The long term context. Quat. Sci. Rev. 134, 1–18. https://doi.org/10.1016/j.quascirev.2015.12.005.

Wilson, R., Wilson, D., Rydval, M., Crone, A., Büntgen, U., Clark, S., Ehmer, J., Forbes, E., Fuentes, M., Gunnarson, B.E., Linderholm, H.W., Nicolussi, K., Wood, C., Mills, C., 2017. Facilitating tree-ring dating of historic conifer timbers using blue intensity. J. Archaeol. Sci. 78, 99–111. https://doi.org/10.1016/j.jas.2016.11.011.

Yasue, K., Funada, R., Kobayashi, O., Ohtani, J., 2000. The effects of tracheid dimensions on variations in maximum density of Picea glehnii and relationships to climatic factors. Trees 14, 223–229. https://doi.org/10.1007/PL00009766.